Stabilization of Soft Lipid Colloids: Competing Effects of Nanoparticle Decoration and Supported Lipid Bilayer Formation

Sushma Savarala,[†] Selver Ahmed,[†] Marc A. Ilies,[‡] and Stephanie L. Wunder[†,*]

[†]Department of Chemistry, College of Science and Technology, Temple University, Philadelphia, Pennsylvania 19122, United States, and [‡]Department of Pharmaceutical Sciences, School of Pharmacy, Temple University, Philadelphia, Pennsylvania 19140, United States

ABSTRACT Stabilization against fusion of zwitterionic lipid small unilamellar vesicles (SUVs) by charged nanoparticles is essential to prevent premature inactivation and cargo unloading. In the present work, we examined the stabilization of DMPC and DPPC SUVs by monolithic silica (SiO_2) nanoparticle envelopment, for SiO_2 with 4−6, 10−20, 20−30, and 40−50 nm nominal diameter. We found that for these soft colloids stabilization is critically dependent on whether fusion occurs between the charged nanoparticles and neutral SUVs to form supported lipid bilayers (SLBs), or whether the reverse occurs, namely, nanoparticle decoration of the SUVs. While SLB formation is accompanied by precipitation, nanoparticle decoration results in long-term stabilization of the SUVs. The fate of the nanosystem depends on the size of the nanoparticles and on the ionic strength of the medium. We found that, in the case of highly charged SiO_2 nanoparticles in water, there is no SUV fusion to SiO_2 for a specific range of nanoparticle sizes. Instead, the negatively charged SiO_2 nanoparticles surround the uncharged SUVs, resulting in electrostatic repulsion between the decorated SUVs, thus preventing their aggregation and precipitation. Addition of millimolar amounts of NaCl results in rapid SLB formation and precipitation. This study has great potential impact toward better understanding the interaction of nanoparticles with biological membranes and the factors affecting their use as drug carriers or sensors.

KEYWORDS: supported lipid bilayers · stabilization of vesicles · halos · colloidal stabilization · nanoparticles · nanoparticle decoration · SUVs

Supramolecular assemblies formed by lipids, especially curved lipid bilayers, are the structures of choice in nature for isolation of life processes and components and for regulating traffic/transport of biomolecules across these boundaries. Artificial phospholipid vesicles formed by mechanical means such as extrusion or sonication—small unilamellar vesicles (SUVs) and large unilamellar vesicles (LUVs)—have the potential to be surrogates for cell membranes and can be used to transport drugs *in vivo* for various therapeutic applications. However, vesicles are often metastable and aggregate and fuse over a period of hours to days.[1,2] The fusion process is undesirable in many cases where the contents need to remain encapsulated in the interior compartment of the vesicles. When SUVs or LUVs are incubated with planar inorganic surfaces or nanoparticles such as silica (SiO_2), similar undesirable cargo leakage/inactivation can occur due to the fusion process of the SUVs to form supported lipid bilayers (SLBs). On the other hand, SUVs containing hydrophobic drugs and membrane proteins in the hydrophobic lipid core, or hydrophilic materials near the polar lipid headgroups, can be deposited as supported lipid bilayers (SLBs), which can form the basis of nanodevices.[3] However, the stability in time[4,5] of nanodevices based on nanoparticle suspensions constitutes a limiting factor of these technologies.

The fusion process between SUVs and surfaces (both planar and spherical) has been investigated in detail and shown to depend on factors such as the charge density of the support,[6] the charge of the lipids, and the ionic strength of the medium.[7] It is well-documented that salt promotes the formation of SLBs.[8,9] However, on nanoparticles, the addition of salt required for SLB formation is often accompanied by aggregation/precipitation of the SLBs.[10,11] The necessity of colloidal stabilization of SUVs and SLBs for their use in drug/gene delivery, in other applications where encapsulation and transport of drugs and enzymes is required, and for the investigation of membrane proteins and processes[12] has motivated research in this area. In the case of nanoparticle-stabilized 1,2-dilauroyl-*sn*-glycero-3-phosphocholine (DLPC) vesicles, the vesicle outer surface was still available for biofunctionalization.[13] For both SUVs and SLBs, stabilization of the suspensions is enhanced by increasing repulsive interactions (steric or electrostatic) between the nanoparticles. In the case of SUVs, chemical

* Address correspondence to slwunder@temple.edu.

Received for review September 29, 2010 and accepted March 7, 2011.

Published online March 07, 2011
10.1021/nn1025884

stabilization methods, such as polymerization of lipid heads or tails, can decrease SUV fusion through decreased mobility of the oligomers compared with the lipid monomers and thus increase stability, although not indefinitely.[14]

In distilled water and at low ionic strength, suspensions composed of both zwitterionic SUVs and nanoparticles have been found to be stable.[11] This may partially be due to the absence of fusion between the SUVs and silica surface, as found experimentally on planar[15] or nanoparticle[11] silica. When zwitterionic SUVs do not form SLBs on nanoparticles in suspension, we can consider the possibility that the reverse can occur, namely, that the nanoparticles can surround the lipid SUVs. It has been suggested that this is due to the electrostatic attraction of the negatively charged nanoparticles with the positively charged N^+ of the P^-—N^+ (phosphorus—nitrogen) dipole of the PC headgroup, which orients the P^-—N^+ dipole perpendicular to the membrane surface; this mechanism is supported by the weaker interactions of cationic nanoparticles with PC lipids, due to repulsion between the N^+ and positively charged nanoparticle surface.[16]

Stabilization of colloids through a mechanism of nanoparticle envelopment has previously been observed in nanoparticle "halos"[17,18] and Pickering emulsions.[19] The process of nanoparticle "haloing"[17,18] has been used to explain the stabilization of "hard" colloids, where all particles are solids. In this case, charged nanoparticles surround neutral micrometer-size spheres, decreasing van der Waals attractions between the microspheres.[20] Stabilization by nanoparticle haloing has been observed for large diameter (570 or 1180 nm), neutral SiO_2 (at pH = 1.5, below the pK_a of SiO_2) microspheres by small (6 nm diameter) highly positively charged zirconia nanoparticles,[20] and the similar stabilization of 500 nm silica spheres by charged 20 nm polystyrene latex spheres.[21]

"Soft" colloids, typically liquid/liquid or gas/liquid emulsions, can be stabilized if nanoparticles, which are preferentially wet by the continuous phase, are added to a two phase system. In these "Pickering" emulsions,[19] the nanoparticles adsorb at the interface between the two phases, preventing coalescence of the dispersed droplets. Amphiphilic Janus particles,[22] in which one-half of the sphere is hydrophilic and the other half is hydrophobic, have more recently been proposed to stabilize emulsions.[23] Of particular interest to the current investigation is the stabilization against fusion (for up to 50 days) of phosphatidylcholine (PC) SUVs with adsorbed anionic 20 nm carboxy-modified polystyrene latex spheres in phosphate buffered saline (PBS).[24,25] Cationic aliphatic amidine PS latex spheres (20 nm) were even better at stabilization since they bound more weakly to the P^-—N^+ (phosphorus—nitrogen: N^+ toward water) dipole of PC, thus avoiding bridging of adjacent particles.[26,27]

In the current investigation, we examined the stabilization of zwitterionic lipid SUVs by charged monolithic SiO_2 nanoparticles. In particular, we evaluated the competitive processes of nanoparticle envelopment of the SUVs by the SiO_2 or, alternatively, the formation of supported lipid bilayers on the SiO_2. The stabilization of SUVs was investigated in deionized water using negatively charged silica nanoparticles with nominal diameters of 4—6, 10—20, 20—30, 40—50, and 100 nm and neutral zwitterionic SUVs of 1,2-dimyristoyl-*sn*-glycero-3-phosphocholine (DMPC) or 1,2-dipalmitoyl-*sn*-glycero-3-phosphocholine (DPPC) with nominal 50, 100, and 200 nm diameters. We examined the impact of several factors that influenced these two competitive processes—the nature and ratio of the components, the ionic strength of the medium, the nanoparticle size, and thus the intrinsic curvature of the support. Addition of only millimolar quantities of NaCl resulted in immediate precipitation.

RESULTS

Stability. Suspensions were prepared by incubating SiO_2 nanoparticles with DMPC above their phase transition temperatures, T_m, in water for 1 h and then keeping them at room temperature (RT). Stability on the time scale of days to weeks was observed for suspensions of nominal 50, 100, and 200 nm DMPC SUVs and nominal 4—6, 10—20, 20—30, 40—50, and 100 nm nanoparticles, at $\#SiO_2/\#SUV_{DMPC}$ ratios ranging from 2 to 50 000; longer times were not investigated. Addition of only millimolar quantities of NaCl resulted in immediate precipitation.

Similarly, suspensions of SiO_2 nanoparticles and DPPC SUVs in water were incubated above T_m for 1 h and subsequently kept at RT. In this case, stability was observed on the order of months for mixtures of nominal 50 nm DPPC SUVs and nominal 4—6, 40—50, and 100 nm SiO_2 nanoparticles at $\#SiO_2/\#SUV_{DPPC}$ ratios of 25, 1.6, and 0.27, respectively. DPPC was chosen for the longer term stability studies since at RT the DPPC SUVs would be in the gel state, where fusion of SUVs to each other occurs more rapidly and, therefore, would more stringently test stability limits. These suspensions were kept for over a year at RT, without noticeable changes in their appearance for many months. After approximately 5 and 8 months, suspensions with 100 nm and 40—50 nm SiO_2, respectively, became unstable and aggregation/precipitation could be observed, but suspensions with 4—5 nm SiO_2 were stable for at least a year. For similar preparations of only DPPC SUVs, aggregation/precipitation occurred over a period of days.

Dynamic Light Scattering. The diameters of the individual components (SiO_2 nanoparticles and DMPC SUVs) were measured separately in water and analyzed using both *z* and volume percent averages, and the results are summarized in Table 1.

For the mixtures of SiO_2 nanoparticles and DMPC SUVs, the *z* and volume average diameters (*D*) measured when the ratio of $\#SiO_2/\#SUV_{DMPC}$ was increased from 1 to *ca.* 50 000, for nominal 4—6 to 40—50 nm SiO_2

TABLE 1. Diameters and Zeta Potentials of SiO_2 Nanoparticles and DMPC SUVs

	nominal Size (nm)	diameter DLS *z*-average (nm)	diameter DLS volume average (nm)	zeta potential (mV)
SiO_2	4−6	5.3 ± 1.6	11.7 ± 1.0	−23.0 ± 1.6,[a] −33.5[b]
	10−20	12.6 ± 1.8	17.2 ± 1.4	−27.9 ± 1.98,[a] −39.0[b]
	20−30	20.3 ± 0.9	25.2 ± 0.8	−33.2 ± 1.26,[a] −49.6[b]
	40−50	41.6 ± 1.1	47.3 ± 1.3	−40.5 ± 1.45,[a] −57.3[b]
	100	102.0 ± 1.9	110.0 ± 1.3	−45.0 ± 1.96,[a] −62.6[b]
SUVs	50	52 ± 2.69	56 ± 2.36	0.09 ± 0.3
	100	96 ± 3.10	104 ± 3.58	0.60 ± 0.56
	200	156 ± 2.98	178 ± 2.59	0.25 ± 1.21

[a] Schmulokowski approximation, in water. [b] At 0.05 mM NaCl, corrected using f(κa); see text for details.

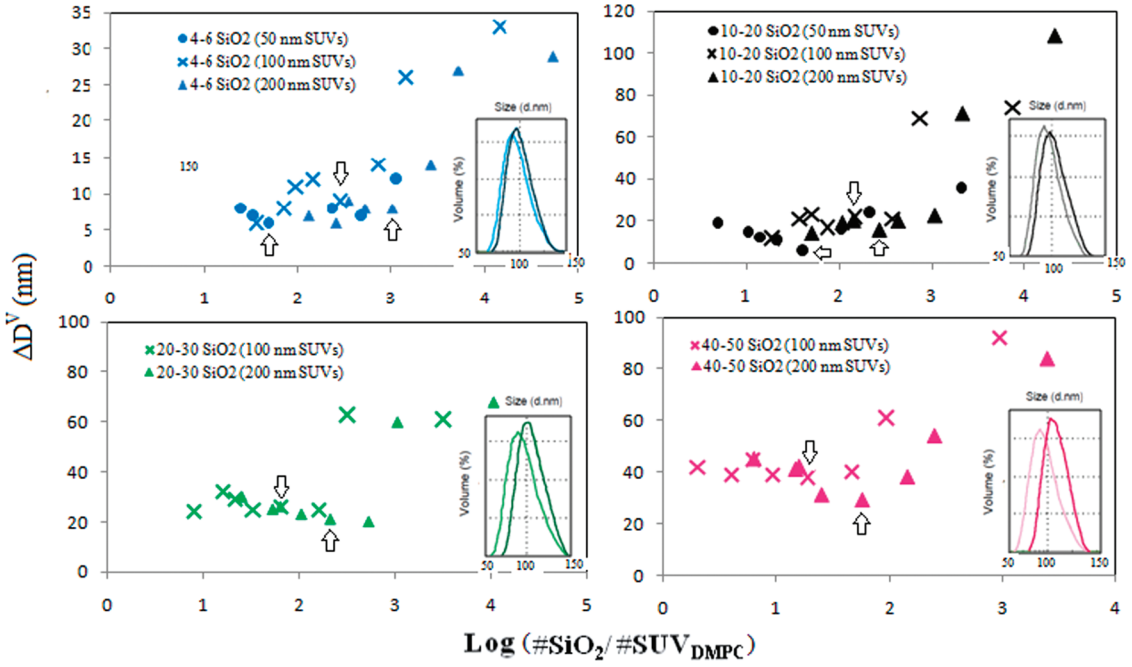

Figure 1. $\Delta D^v = D^v_{SUV+SiO_2} - D^v_{SiO_2}$ *versus* log (#SiO_2/#SUV_{DMPC}). $D^v_{SUV+SiO_2}$ corresponds to the diameter of the SiO_2 decorated DMPC SUVs, and $D^v_{SiO_2}$ corresponds to the diameter of the SiO_2 nanoparticles, both measured as the volume average by DLS. Values of ΔD^v are plotted for the nominal 4−6 and 10−20 nm SiO_2 from nominal 50, 100, and 200 nm SUVs. Values of ΔD^v are plotted for the nominal 20−30 and 40−50 nm SiO_2 from the nominal 100 and 200 nm SUVs. Arrows correspond to calculated values of #SiO_2/#SUV_{DMPC} where the silica would form a close-packed layer around the SUVs. Insets show typical (color-coded) DLS data for the nanoparticles, $D^v_{SiO_2}$ (light line), and decorated $D^v_{SUV+SiO_2}$ (dark line).

and nominal 50, 100, and 200 nm DMPC SUVs, are presented more fully in Supporting Information (Tables IA, IB, and IC for the nominal 50, 100, and 200 nm DMPC SUVs, respectively).

Analysis of the data from Supporting Information Tables IA, IB, and IC indicates that at values of #SiO_2/#SUV_{DMPC} <100 (or greater depending on D_{SUV}/D_{SiO_2}), the *z*-average size, which is weighted by the intensity of the scattering species and that in turn scales as the sixth power of the radius, is *higher* than the size of the neat DMPC SUVs. These results strongly suggest that the nanosystem is not a simple combination of DMPC SUVs and SiO_2 nanoparticles since adding smaller particles to larger particles would decrease the *z*-average size. The *z*-average size does eventually decrease as #SiO_2/#SUV_{DMPC} increases: as more SiO_2 nanoparticles are added, the *z*-average diameters decrease due to the large number of smaller scatterers. The value of #SiO_2/#SUV_{DMPC} at which the *z*-average size begins to decrease is a function of D_{SUV}/D_{SiO_2}, due to the r^6 dependence of the scattering intensity on particle size.

When the mixtures of SiO_2 nanoparticles and DMPC SUVs are analyzed by volume, an algorithm[28] corrects for differences in scattering power for materials of different size using Mie scattering theory. The neat SiO_2 nanoparticles and DMPC SUVs always exhibit scattering from a single species (Table 1). In mixtures of SUVs and SiO_2 nanoparticles at small values of #SiO_2/#SUV_{DMPC} (Supporting Information Tables IA, IB, and IC), there is also only a single scattering species, which however has a larger diameter (volume average) than the original DMPC SUVs. The insets in Figure 1 show examples of the DLS data for the 100 nm DMPC SUVs alone and the 100 nm SUVs incubated with nominal 4−6, 10−20, 20−30, and 40−50 nm SiO_2 nanoparticles.

As $\#SiO_2/\#SUV_{DMPC}$ increases, two scattering species can be clearly distinguished (see Supporting Information Tables IA, IB, and IC). The diameter of one of the scatterers corresponds to that of free, unassociated SiO_2 nanoparticles, $D^v_{SiO_2}$, where the superscript v indicates that volume analysis was used. Values of $D^v_{SiO_2}$ (*measured when two scattering species are present*) agree well with the diameters by volume obtained when the nominal 4−6, 10−20, 20−30, and 40−50 nm SiO_2 nanoparticles are measured alone (Table 1). The diameters, $D^v_{SUV+SiO_2}$, of the other scattering species are attributed to DMPC SUVs increased in size by the surrounding nanoparticles and will be referred to as "decorated" SUVs (*vide infra*). The increase in diameter of the DMPC SUVs due to the associated SiO_2 is $\Delta D^v = D^v_{SUV+SiO_2} - D^v_{SiO_2}$. Plots of ΔD^v *versus* log $(\#SiO_2/\#SUV_{DMPC})$ are presented in Figure 1a−d for the individual 4−6, 10−20, 20−30, and 40−50 nm SiO_2, in mixtures with nominal 50, 100, and 200 nm DMPC SUVs, respectively. The graphs show that the diameter increase correlates directly with the nanoparticle size, independent of the size of the DMPC SUVs. At low values of $\#SiO_2/\#SUV_{DMPC}$, the size increase ΔD^v is approximately one nanoparticle diameter, namely, 8.6 ± 1.5, 17.5 ± 2.5, 28.2 ± 1.1, and 40.2 ± 0.4 nm for the nominal 4−5, 10−20, 20−30, and 40−50 nm SiO_2, and agrees well with the values for the nanoparticles measured separately (see Table 1). As $\#SiO_2/\#SUV_{DMPC}$ increases, ΔD^v approximately doubles in value. As discussed below (*vide infra*), we suggest that this occurs due to increased stiffening of the SUVs as more SiO_2 nanoparticles adsorb to the lipid bilayer.

The calculated ratios of $\#SiO_2/\#SUV_{DMPC}$ at which the nanoparticles would form a geometrically close-packed arrangement are indicated by arrows in the Figure 1a−d and are near but below where the doubling of ΔD^v is observed. This is expected since not all of the added SiO_2 nanoparticles envelop the SUVs; SiO_2 nanoparticles are also free in the suspension.

When the DLS data are analyzed by volume, the percentage of the populations of the species is also indicated (Supporting Information Tables IA, IB, and IC). We postulate that when two species are present, the system is composed of the SiO_2 nanoparticles themselves and the SiO_2 decorated SUVs (*vide infra*). The percentages of both the SiO_2 nanoparticles and SiO_2 decorated SUVs are plotted as a function of $\log(\#SiO_2/\#SUV_{DMPC})$ in Figure 2a−c for the nominal 50, 100, and 200 nm SUVs, respectively, mixed with 4−6, 10−20, 20−30, and 40−50 nm SiO_2. At low $\#SiO_2/\#SUV$ values, only diameters corresponding to SiO_2 decorated SUVs are observed. As $\#SiO_2/\#SUV_{DMPC}$ increases, both SiO_2 nanoparticles and SiO_2 decorated SUVs are detected, with the percentage of SiO_2 decorated nanoparticles decreasing and that of the nanoparticles themselves increasing, as expected. Two populations are observed at slightly smaller $\#SiO_2/\#SUV_{DMPC}$ for larger nanoparticles for each DMPC SUV size and for smaller DMPC SUVs at the same nanoparticle size since smaller numbers of nanoparticles of larger size are required to decorate a given size DMPC SUV.

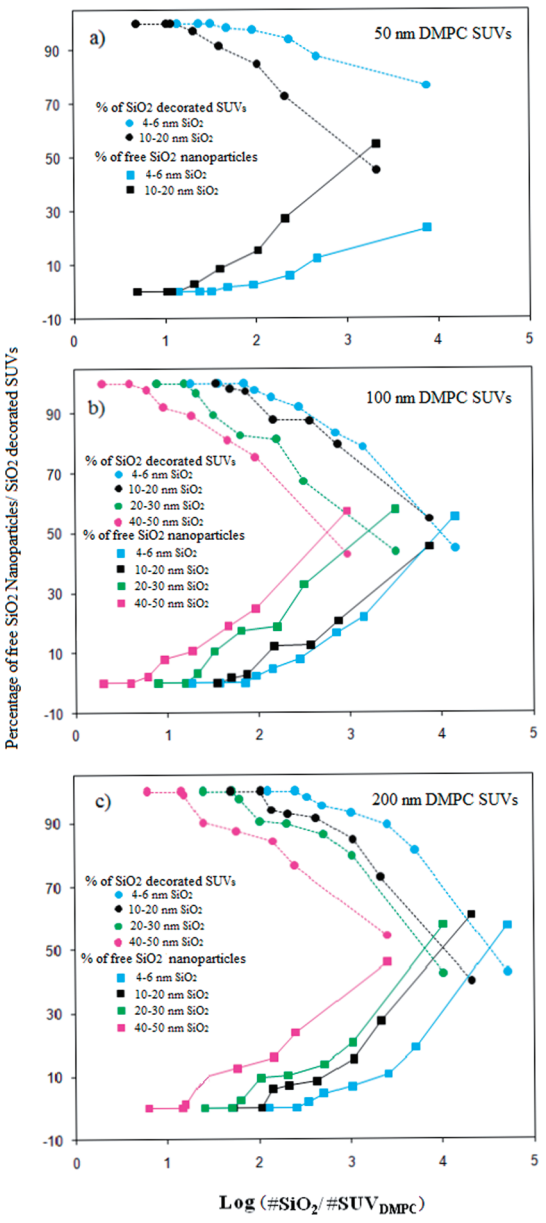

Figure 2. Percent of nanoparticles and SiO_2 decorated DMPC SUVs obtained from DLS volume averages for nominal: (a) 50 nm; (b) 100 nm; (c) 200 nm DMPC SUVs as a function of $\log(\#SiO_2/\#SUV_{DMPC})$, in water.

Zeta Potential Measurements. The zeta potentials of the nanoparticles and SUVs are presented in Table 1. The zwitterionic DMPC SUVs have zeta potentials of around zero within experimental error. Although the isoelectric point of egg phosphatidylcholine (PC) is 4.13,[29] suggesting that DMPC with the same zwitterionic headgroup would have a slightly negative charge at pH = 8; this does not seem to be the case here. The zeta potentials of the SiO_2 nanoparticles themselves decrease with decreasing size.[30]

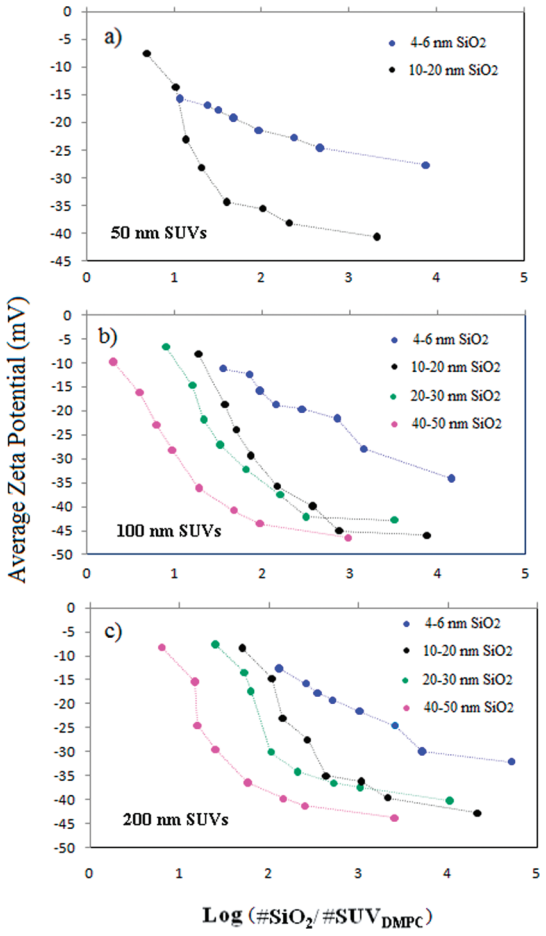

Figure 3. Average zeta potential data for suspensions of nominal (a) 50, (b) 100, and (c) 200 nm DMPC SUVs and 4−6, 10−20, 20−30, and 40−50 nm SiO_2 nanoparticles in water as a function of log(#SiO_2/#SUV_{DMPC}).

For each DMPC SUV of nominal 50, 100, and 200 nm diameter, average zeta potential data are plotted as a function of #SiO_2/#SUV_{DMPC} in Figure 3. At small values of #SiO_2/#SUV_{DMPC}, low negative values of the zeta potential are observed for all DMPC SUVs, indicating that the SiO_2 nanoparticles surround the neutral SUVs and move as a single species with lower charge density. With increasing #SiO_2/#SUV_{DMPC}, average zeta potentials increase and approach the zeta potentials of the pure nanoparticles. The Schmulokowski approximation was used in all cases since the DLS data indicated the existence of large complex species (decorated SUVs). For very large values of #SiO_2/#SUV_{DMPC}, where there is a large excess of nanoparticles, the zeta potential of the system is close to that of the SiO_2 nanoparticles themselves (Table 1).

TEM. For direct visualization of the structure of the nanosystem comprising SiO_2 nanoparticles and DMPC SUVs, we obtained TEM micrographs of the 10−20 nm SiO_2 and nominal 100 nm DMPC SUVs prepared in water for #SiO_2/#SUV_{DMPC} = 38/1 and 150/1 (Figure 4). The stained lipids can be observed in the TEM images. For #SiO_2/#SUV_{DMPC} = 38/1, SiO_2 nanoparticles can be observed around the SUVs and in the surrounding area. Further, the SUVs have oblate shapes. By contrast, for #SiO_2/#SUV_{DMPC} = 150/1 (a value for which the SiO_2 would form a close-packed layer around the SUVs), there were more SiO_2 nanoparticles surrounding the SUVs (approximately twice as many) as well as in the surrounding area, and the SUVs looked spherical. The dimensions of the SUVs are less than the nominal diameter of the 100 nm SUVs. This can arise due to shrinkage of the SiO_2 decorated SUVs on the TEM grid

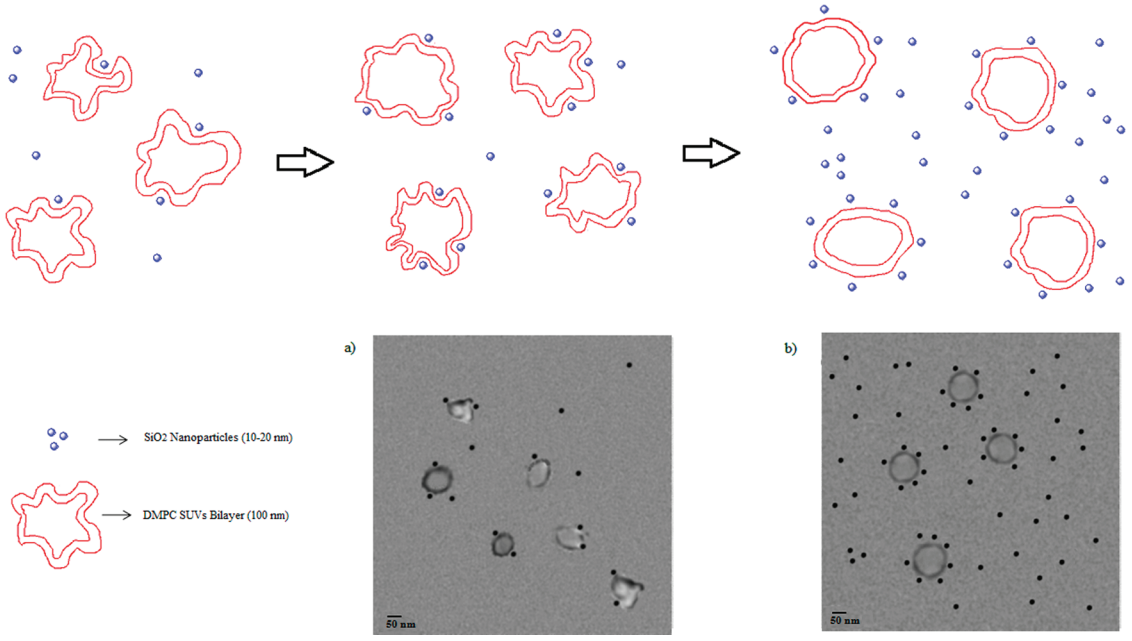

Figure 4. (Top) Schematic of formation (left to right) of "decorated" SUVs, when SUV diameter is unchanged, increased by *ca.* 1 or 2 right nanoparticle diameters; (bottom) TEM micrographs for nominal 10−20 nm SiO_2 prepared with nominal 100 nm SUVs for #SiO_2/#SUV_{DMPC} = 38/1 (bottom left) and 150/1 (bottom right).

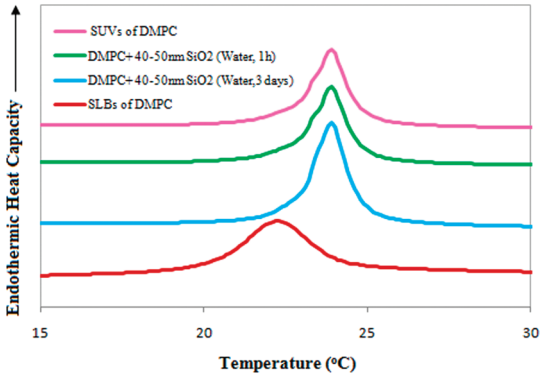

Figure 5. Nano-DSC thermograms of nominal 100 nm DMPC SUVs incubated with nominal 40−50 SiO_2 (1 h/40 °C): stable suspensions of SUVs in water for 1 h or 3 days, and precipitated SLBs in 10 mM NaCl.

or because the image was captured for a decorated SUV at an off-diameter position.

Nano-DSC. In order to gain more insight into the morphology and dynamics of systems comprised of DMPC SUVs and SiO_2 nanoparticles of different sizes, nano-DSC scans were run after incubation at 40 °C for 1 h and kept at RT for up to 4 days. Nano-DSC traces can differentiate between SUVs and SLB since, for DMPC SLBs, the gel to liquid phase transition temperature is decreased by 2 °C compared with the SUVs.[10,11] Figure 5 shows nano-DSC thermograms of the original 100 nm SUVs and the 100 nm SUVs incubated with nominal 40−50 nm SiO_2 in water at RT. All of the thermograms are identical to each other and clearly display no evidence of SLB formation. Only the gel to liquid crystal transitions indicative of SUVs were observed on both the heating (T_m) and cooling (T_c) cycles for DMPC suspensions of 50, 100, and 200 nm SUVs incubated in water (1 h at 40 °C) with the 4−6, 10−20, 20−30, and 40−50 nm SiO_2 and kept at RT for *ca.* 4 days (the longest time investigated). By contrast, addition of millimolar amounts of NaCl resulted in SLB formation (Figure 5) and immediate precipitation.

DISCUSSION

The colloidal stability of phospholipid vesicles is not adequately described using the Derjaguin−Landau−Verwey−Overbeek (DLVO) theory, in which only long-range van der Waals attractions and electrostatic repulsion (double layer forces) are considered. Although at large distances (*ca.* 50 Å in water[31,32]) DLVO theories are in good agreement with experiment,[33,34] at smaller distances (*ca.* 1−2 nm), other short-range repulsive forces exist between two approaching hydrophilic surfaces in water. These short-range interactions have been attributed to (i) hydration forces, that is, the energy needed to dehydrate interacting surfaces that contain ionic or polar species;[35] (ii) thermal undulation;[36,37] and (iii) protrusion[38] forces. Colloidal stability is achieved when the combination of particle−particle interactions due to longer range screened electrostatic repulsive interactions, attractive intermediate range van der Waals interactions, and short-range (steric, solvation, undulation, protrusion) interactions is repulsive at all particle−particle separations or results in a repulsive energy barrier that is too high to cross due to thermal fluctuations and forces of gravitational origin on relevant time scales.

In this work, a process of nanoparticle "decoration" (in which SiO_2 nanoparticles surround SUVs) can be used to explain the remarkable colloidal stability of zwitterionic DMPC and DPPC SUVs over periods of months in the presence of negatively charged SiO_2 nanoparticles. As discussed below, in general, this occurs when SUVs mixed with SiO_2 nanoparticles do not fuse to the nanoparticles to form SLBs, and instead the nanoparticles surround and decorate the exterior of the SUVs. A theoretical model[17,18] of nanoparticle haloing of charged nanoparticles around larger neutral microspheres has been used to explain the behavior of hard sphere colloids, and ideas from this model can be used to explain the present stabilization of soft colloids of neutral SUVs decorated with negatively charged nanoparticles.

Nanoparticle-induced stabilization can arise from relatively weak van der Waals attraction between the colloid and the nanoparticles,[39] but Monte Carlo simulations of halos indicate that a dramatic enhancement of the stabilization occurs for longer range colloid−nanoparticle attractions.[40] It is well-known that in water the interaction between zwitterionic vesicles and silica is due to longer range electrostatic forces[15] and results in adsorption, but not typically fusion, of the vesicles to the surface. In the current investigation, the relatively strong attraction between the DMPC and DPPC zwitterionic lipids and SiO_2 in water was indicated by their partial fusion on larger 100 nm nanoparticles.[11]

We describe the association of the nanoparticles around the SUVs as "decorations" for two reasons. On the one hand, halos imply that a distance separates the SUV and nanoparticle surfaces, for which we have no experimental evidence. Halos have been observed for the zirconia/SiO_2 system, where a distance of approximately 2 and 2.3 nm was measured between the zirconia nanoparticles and micrometer-size SiO_2 spheres by ultra-small-angle X-ray scattering[41] and transition force measurements,[42] respectively. On the other hand, fusion does not occur between the DMPC SUVs and nanoparticles of nominal 4−6 to 40−50 nm diameter size in water, as evidenced by the lack of a SLB peak in the nano-DSC traces. However, the formation of DMPC SLBs on the larger 100 nm SiO_2 in water as a function of time strongly indicates adsorption of the zwitterionic lipids on the SiO_2, even in the absence of salt.[11] Further, the TEM traces, which show

nanoparticle circles around the SUVs, suggest that the nanoparticles were adsorbed to the SUVs; it was this adsorption that might have held the nanoparticles as ordered spheres after evaporation of water from the TEM grids.

The stability of the zwitterionic lipid SUVs and SiO_2 nanoparticles in water is consistent with a process in which as the negatively charged SiO_2 are added to the suspension they tend to minimize their nearest neighbor distances and segregate toward the neutral SUVs, shown schematically in Figure 4 top. The electrostatic repulsion between the charged nanoparticles surrounding the neutral SUVs is the most likely cause for the inability of the SUVs in water to aggregate. The processes involved as $\#SiO_2/\#SUV_{DMPC}$ increases and ordered "decorations" around the SUVs are formed are believed to occur as follows:

(i) At low $\#SiO_2/\#SUV_{DMPC}$, the charged SiO_2 migrates toward the neutral SUVs. The single-ζ potential (which increases as more SiO_2 is added) and size reflect the movement of a single species, namely, that consisting of the DMPC SUVs surrounded by increasing amounts of the charged SiO_2 nanoparticles. In the case of neutral SiO_2 microspheres surrounded by zirconia nanoparticles, the approach of ζ to that of the estimated value of pure nanoparticles (+65 mV) was interpreted to show that the two species moved cooperatively together since the electrophoretic mobility of charged species is size independent.[20]

(ii) Eventually, the charged SiO_2 nanoparticles repel each other laterally, so that there is a limit to the number of SiO_2 directly associated and moving with the DMPC SUVs. This "open structure" was directly observed by TEM images. Halos are predicted to be in a non-close-packed arrangement at stabilization,[40] and it has been shown by ultra-small-angle X-ray scattering that the lateral separation distance between nanoparticles with a halo greatly exceeded their characteristic size.[41] This same charge repulsion between the SiO_2 nanoparticle "decorations" should also result in a non-close-packed arrangement around the SUVs.

(iii) As $\#SiO_2/\#SUV_{DMPC}$ increases, two diameters are measured by DLS, which reflect the two species present, namely, the DMPC SUVs surrounded by the SiO_2 nanoparticles and the isolated "free" SiO_2 nanoparticles themselves. Since the size of the SiO_2 decorated SUVs initially increased by only a single nanoparticle diameter, we postulate that, at this stage, the DMPC SUVs were sufficiently mobile so that structures shown in Figure 4 top, as well as in the TEM images, are present.

(iv) With further increase in $\#SiO_2/\#SUV_{DMPC}$, the size of the SiO_2 decorated DMPC SUVs increases to a value corresponding to *ca.* 2 nanoparticle diameters. We postulate that the added SiO_2 adsorbed to the DMPC SUVs stiffens the SUV bilayer, which results in the more spherical structures represented schematically in Figure 4 top and shown in the TEM images. In this case, the measured diameters of the SiO_2 decorated SUVs now reflect the size expected if SiO_2 of a particular size (4−6, 10−20, 20−30, 40−50 nm) enveloped the SUVs (*i.e.*, $2D_{SiO_2}$). The ratio ($\#SiO_2/\#SUV_{DMPC}$) at which this change occurs increases with a decrease in SiO_2 size, indicating, as might be expected, that a greater number of smaller SiO_2 nanoparticles can be accommodated around the same number of SUVs (Figure 1).

(v) Finally, $\#SiO_2/\#SUV_{DMPC}$ becomes so large (the free, isolated SiO_2 become so numerous) that the zeta potential has a value approximately that of the neat SiO_2. However, two size species are still observed by DLS. This indicates that both of the species, the free, isolated nanoparticles and the decorated SUVs have similar zeta potentials.

Models of colloidal stabilization by haloing suggest that there will be phase separation at both low and high concentrations of the smaller particles in binary mixtures of spheres, and that this phase separation will depend on the relative size of the two size spheres. In the current investigation, although three regimes might be expected, namely, aggregation of the neutral spheres (DMPC SUVs) at low nanoparticle concentrations by van der Waals attractions, stabilization at intermediate concentrations by decoration, and aggregation at higher nanoparticle concentrations as the result of entropic[43,44]/repulsive[17,26] depletion[45] or bridging interactions,[21,40,46] we observed only nanoparticle decoration. Unlike other systems reported in the literature, where the "large" micrometer-size particles were neutral SiO_2 and the small charged particles were nanometer size,[20] we did not observed fast (<1 min) flocculation at either high or low volume fractions of the nanoparticles.

The lack of aggregation on short time scales observed here, at any concentration of nanoparticles, may occur because these are soft colloids. Undulation/protrusion repulsive forces exist for the SUVs that result in effective short-range repulsions, which would not be expected for the hard silica microspheres. In addition, both the SUVs and SiO_2 separately exhibit longer-term stability: the process of vesicle fusion for the SUVs that results in aggregation/precipitation can take days, and the SiO_2 nanoparticles have been extensively dialyzed (as indicated by the manufacturer)

so that aggregation can take months. Lastly, the volume fraction (ϕ) of nanoparticles used here was low ($\phi \approx 4 \times 10^{-4}$ to 4×10^{-3}).

For these soft colloids, fast aggregation/precipitation is associated principally with the formation of SLBs on the nanoparticles. The addition of even small amounts of salt (ionic strengths >0.75 mM NaCl) to stable suspensions of 4−6 to 100 nm SiO_2/DMPC SUVs, triggers the *formation of SLBs and their rapid flocculation/precipitation*.[11] The precipitation is due to shielding of the electrostatic charge of the SiO_2 by the lipids and salt and by suppression of undulatory/protrusion forces of lipids on solid substrates. Once the lipids fuse to the nanoparticles, the only force keeping the SLBs apart is their electrostatic repulsion, and the charge on the SiO_2 is shielded by the zwitterionic lipids and the added salt, weakening this repulsive interaction. However, when excess SUVs are present, the undulatory/protrusion forces can be restored, and the SLBs resuspended.[30]

Our observations are most closely related to those reported for the stabilization against fusion of 100−400 nm 1,2-dilauroyl-*sn*-glycero-3-phosphocholine (DLPC) by 20 nm negatively charged carboxyl-modified polystyrene (PS) spheres in PBS buffer.[24] It is possible that, for this system, the DLPC cannot form SLBs around the negatively charged 20 nm carboxyl-modified PS spheres. This may arise due to the small diameter of the nanoparticles since it has been shown that *ca.* 20 nm is the cutoff for the formation of SLBs[11,47] and/or to the low charge density of the PS since zwitterionic lipids have been shown to form SLBs on both positively and negatively charged surfaces only when there is sufficient charge density (*ca.* >80%).[6] In this context, we note that SLB formation of DMPC onto SiO_2 nanoparticles was shown to depend on both nanoparticle size and ionic strength. Higher ionic strengths were required for fusion of DMPC onto smaller diameter SiO_2.[11]

CONCLUSIONS

The stabilization of suspensions of negatively charged SiO_2 nanoparticles of 4−6 to 40−50 nm nominal size and zwitterionic DMPC or DPPC small unilamellar vesicles (SUV) of nominal 50−200 nm diameter was found to depend on whether the SUVs fused to the SiO_2 to form supported lipid bilayers (SLBs) or remained as separate SUVs and SiO_2 nanoparticles. In water, there was no SLB formation for the 4−6 to 40−50 nm SiO_2. In this case, stabilization of the suspensions occurred by a mechanism of nanoparticle decoration of the SUVs by the charged SiO_2 nanoparticles. The negatively charged SiO_2 surrounded the uncharged zwitterionic SUVs and resulted in electrostatic repulsion between the SiO_2 decorated SUVs preventing their aggregation and precipitation. The persistence of SUVs was evidenced by nano-DSC thermograms that only showed gel-to-liquid crystal transition temperatures (T_m) characteristic of SUVs. The formation of SiO_2 envelopes around SUVs was directly visualized by TEM micrographs. DLS and zeta potential data indicated that, as $\#SiO_2/\#SUV_{DMPC}$ increased, the nanoparticles surrounded the DMPC SUVs and eventually two populations, one of SiO_2 decorated SUVs and the other of free SiO_2 nanoparticles, could be distinguished. The suspensions were stable over a large range of investigated compositions, from $\#SiO_2/\#SUVS$ = 1 to 50 000 and times of up to a year. The addition of even small amounts of salt (≥0.75 mM NaCl) caused rapid disruption of the SUVs, supported lipid bilayer formation, and concomitant aggregation/precipitation of the SLBs. This process can form the basis of a simple method of releasing the contents of the vesicles. The mechanisms discussed above may constitute a new way to stabilize vesicles and at the same time provide the experimental foundation for a new type of imaging or delivery system. Further elucidation of the factors affecting stabilization or precipitation of SUVs and SLBs will help in understanding the interaction and fate of nanoparticles with cell membranes, with implications toward understanding nanoparticle toxicity and biodegradation, and the factors that can trigger physiological processes such as endocytosis.

EXPERIMENTAL SECTION

Materials. 1,2-Dimyristoyl-*sn*-glycero-3-phosphocholine (DMPC, 14:0 PC) and 1,2-dipalmitoyl-*sn*-glycero-3-phosphocholine (DPPC, 16:0 PC) were obtained from Avanti Polar Lipids (Alabaster, AL) and used without further purification. Snowtex colloidal silica (SiO_2) nanoparticle suspensions, with densities of 2.2−2.6 g/cm^3 (reported by manufacturer) and prepared by a water glass process, were a gift from Nissan Chemical America (Houston, TX). The nominal diameters were (i) 4−6 nm, ST-XS, 20.3 wt % SiO_2, lot 150509, pH 9.2, specific gravity 1.135; (ii) 10−20 nm, ST-40, 40.8 wt % SiO_2, lot 170916, pH 10.1, specific gravity 1.308; (iii) 20−30 nm, ST-50, 47.9 wt % SiO_2, lot 170418, pH 8.9, specific gravity 1.372; (iv) 40−50 nm, ST-20 L, 20 wt % SiO_2, lot 170211, pH = 9.5−11.0, specific gravity 1.12−1.14; and (v) 100 nm, MP-1040, 40.7 wt % SiO_2, lot 170425, pH 9.3, specific gravity 1.300. All solutions/suspensions were prepared with either chloroform ($CHCl_3$) or HPLC grade water, with or without NaCl. All reagents were purchased from Fisher Chemicals (Fairlawn, NJ). An Avanti Mini-Extruder from Avanti Polar Lipids was employed for extrusion of the lipids, using 50, 100, or 200 nm pore size polycarbonate filters.

Methods/Techniques. *Preparation of Suspensions.* Appropriate amounts of lipid were dissolved in chloroform. Dry lipid films were formed after evaporation of the $CHCl_3$ solutions under a stream of nitrogen and then in a vacuum oven overnight to remove any residual solvent. The lipid film was subsequently

redispersed in water and incubated at temperatures (40−60 °C) above the T_m values of the DMPC and DPPC, for a minimum of 2 h with periodic shaking to form hydrated multilamellar vesicles (MLVs). Small unimolecular vesicles (SUVs) were obtained from MLVs by subjecting them to five freeze/thaw cycles followed by extrusion using polycarbonate filters with 50, 100, and 200 nm pores. Approximately 1 mL of a 5−10 mg/mL lipid solution was passed back and forth for up to 50 times. Although a clear solution was obtained after 20 passes, the vesicles became more monodisperse as the number of passes increased (as determined by dynamic light scattering data; see below). Assuming no loss of lipid during the extrusion process, we added additional water or salt solution to the extrusion product to yield vesicle solutions of ~2 mg/mL lipid.

The vesicles and nanobeads were mixed and incubated above the T_m (24 °C for DMPC and 41 °C for DPPC) for 1 h and then kept at RT. The relative amount of lipid and SiO_2 is reported as the number of SiO_2 nanoparticles compared with the number of SUVs (#SiO_2/#SUVs), based on diameters ($D_{SiO_2} = 2R_{SiO_2}$ or $D_{SUV} = 2R_{SUV}$) determined from DLS data; the formula and calculations are given in Supporting Information Tables IA, IB, and IC. Alternatively, the amount of lipid required to achieve single bilayer coverage was calculated using the surface area occupied by the lipid headgroup (0.59 nm^2 for DMPC and 0.63 nm^2 for DPPC[48]) and the total surface area of the nanoparticles, with the assumption that the latter was a planar surface (this implies that the headgroups pack as they would on a planar surface, but that the tails splay) and using a value for the density of 2.4 g/cm^3. The amount of lipid required for single bilayer coverage of the nanoparticles is achieved when the surface area of the SUVs (SA_{SUV}) was equal to the surface area of the SiO_2 (SA_{SiO_2}), $SA_{SUV}/SA_{SiO_2} = 1$, with other amounts given as fractions or multiples of bilayer coverage. This information is presented in detail in Tables IA, IB, and IC of the Supporting Information. Size ratios $\eta = R_{SUV}/R_{SiO_2} = 2.2$ to 16 and mole fractions $SiO_2/(SiO_2 +$ SUVs) between 0.705 to 1 and 0.992 to 1 were used for the DLS and zeta potential measurements for the nominal 50, 100, and 200 nm DMPC SUVs. The volume fractions (ϕ) of the suspensions were $\phi \approx 4 \times 10^{-4}$ to 4×10^{-3} for nanoparticles and $\phi \approx 2 \times 10^{-5}$ to 3×10^{-2} for SUVs.

Analysis. *DLS and Zeta (ζ) Potentials.* Dynamic light scattering (DLS) and zeta (ζ) potential measurements were obtained on a Malvern (Malvern Instruments Ltd. Malvern, U.K.) Zetasizer Nano-ZS at 25 °C, illuminating the sample with 633 nm wavelength radiation from a solid-state He−Ne laser and collecting the scattered light at an angle of 170°. The SiO_2 nanoparticle suspensions were used as received without adjustment in the pH. Diameters are reported either as *z* or volume averages. Both *z* and volume averages were calculated based on nonlinear least-squares (NLLS) fits of the autocorrelation function with Malvern's Zetasizer Nano 4.2 software utilizing a version of the CONTIN algorithm.[28] The resultant correlation function can be analyzed using two different algorithms. The first one (cumulants analysis, defined in ISO13321[28]) determines the mean decay rate and produces a mean diameter (*z*-average diameter) and an estimate of the width of the distribution (the polydispersity index, PDI). The second approach is to fit a multiexponential to the correlation function in order to obtain a distribution of diffusion coefficients (and hence a distribution of particle sizes which are based upon the intensity of scattered light; the distribution is therefore an intensity particle size distribution (PSD)). Conversion of the fundamental intensity PSD information into volume is performed using Mie theory.[28] Zeta potential measurements were obtained in disposable capillary (DTS1060) or dip cells, where the applied voltage was 30 V/cm in the former and 3−5 V/cm in the latter case. The Smoluchowski approximation was used to convert mobilities into ζ potentials for the decorated SUVs. For the SiO_2 nanoparticles, values of the ζ potential corrected using f(κa) in 0.05 mM NaCl (κ^{-1} is Debye screening length, *a* is particle radius), as described elsewhere,[30] are also reported.

Nanodifferential Scanning Calorimetry (Nano-DSC). Nanodifferential scanning calorimetry (nano-DSC) measurements were obtained on a TA Instruments (New Castle, DE) Nano DSC-6300. Samples were scanned at heating/cooling rates of 1 °C/min, using 1−2 mg of total lipid in the analyzed samples (750 μL analyzed volume).

TEM. TEM measurements were made on a FEI Technai 12T electron microscope with an operating voltage of 120 KeV. Samples were prepared with #SiO_2/#SUV_{DMPC} = 38/1 and 150/1. In both cases, 2 μL of the suspensions (20 wt % SiO_2) was placed on carbon-coated, type-A 300 mesh copper TEM grids (Ted Pella, Inc., Redding, CA), the excess water wicked away, and the grids air-dried for 10−15 min. Images were captured using a Gatan DualVision 300 (1k), side-entry cooled CCD camera. Image capture, processing, and analysis were performed with Gatan "Digital Micrograph" software.

Acknowledgment. The support of a SEED grant from Temple University Office of the Provost is gratefully acknowledged. We also thank Dr. F. Monson of Westchester University for assistance in obtaining the TEM images.

Supporting Information Available: Tables IA−IC. This material is available free of charge *via* the Internet at http://pubs.acs.org.

REFERENCES AND NOTES

1. Szoka, F.; Papahadjopoulos, D. Comparative Properties and Methods of Preparation of Lipid Vesicles (Liposomes). *Annu. Rev. Biophys. Bioeng.* **1980,** 467–508.
2. Lei, G. H.; MacDonald, R. C. Lipid Bilayer Vesicle Fusion: Intermediates Captured by High-Speed Microfluorescence Spectroscopy. *Biophys. J.* **2003,** *85*, 1585–1599.
3. Anrather, D.; Smetazko, M.; Saba, M.; Alguel, Y.; Schalkhammer, T. Supported Membrane Nanodevices. *J. Nanosci. Nanotechnol.* **2004,** *4*, 1–22.
4. Bayerl, T. M. A Glass Bead Game. *Nature* **2004,** *427*, 105–106.
5. Baksh, M. M.; Jaros, M.; Groves, J. T. Detection of Molecular Interactions at Membrane Surfaces through Colloid Phase Transitions. *Nature* **2004,** *427*, 139–141.
6. Cha, T.; Guo, A.; Zhu, X. Y. Formation of Supported Phospholipid Bilayers on Molecular Surfaces: Role of Surface Charge Density and Electrostatic Interaction. *Biophys. J.* **2006,** *90*, 1270–1274.
7. Richter, R. P.; Berat, R.; Brisson, A. R. Formation of Solid-Supported Lipid Bilayers: An Integrated View. *Langmuir* **2006,** *22*, 3497–3505.
8. Boudard, S.; Seantier, B.; Breffa, C.; Decher, G.; Felix, O. Controlling the Pathway of Formation of Supported Lipid Bilayers of DMPC by Varying the Sodium Chloride Concentration. *Thin Solid Films* **2006,** *495*, 246–251.
9. Seantier, B.; Kasemo, B. Influence of Mono- and Divalent Ions on the Formation of Supported Phospholipid Bilayers *via* Vesicle Adsorption. *Langmuir* **2009,** *25*, 5767–5772.
10. Ahmed, S.; Wunder, S. L. Effect of High Surface Curvature on the Main Phase Transition of Supported Phospholipid Bilayers on SiO_2 Nanoparticles. *Langmuir* **2009,** *25*, 3682–3691.
11. Savarala, S.; Ahmed, S.; Ilies, M.; Wunder, S. L. Formation and Colloidal Stability of DMPC Supported Lipid Bilayers on SiO_2 Nanobeads. *Langmuir* **2010,** *26*, 12081–12088.
12. Troutier, A. L.; Ladaviere, C. An Overview of Lipid Membrane Supported by Colloidal Particles. *Adv. Colloid Interface Sci.* **2007,** *133*, 1–21.
13. Zhang, L. F.; Dammann, K.; Bae, S. C.; Granick, S. Ligand−Receptor Binding on Nanoparticle-Stabilized Liposome Surfaces. *Soft Matter* **2007,** *3*, 551–553.
14. Chiruvolu, S.; Israelachvili, J. N.; Naranjo, E.; Xu, Z.; Zasadzinski, J. A.; Kaler, E. W.; Herrington, K. L. Measurement of Forces between Spontaneous Vesicle-Forming Bilayers. *Langmuir* **1995,** *11*, 4256–4266.
15. Anderson, T. H.; Min, Y. J.; Weirich, K. L.; Zeng, H. B.; Fygenson, D.; Israelachvili, J. N. Formation of Supported Bilayers on Silica Substrates. *Langmuir* **2009,** *25*, 6997–7005.
16. Yu, Y.; Anthony, S. M.; Zhang, L. F.; Bae, S. C.; Granick, S. Cationic Nanoparticles Stabilize Zwitterionic Liposomes Better than Anionic Ones. *J. Phys. Chem. C* **2007,** *111*, 8233–8236.

17. GaribayAlonso, R.; MendezAlcaraz, J. M.; Klein, R. Phase Separation of Binary Liquid Mixtures of Hard Spheres and Yukawa Particles. *Physica A* **1997,** *235*, 159–169.
18. Chavez-Paez, M.; Gonzalez-Mozuelos, P.; Medina-Noyola, M.; Mendez-Alcaraz, J. M. Correlations among Colloidal Particles Confined to a Spherical Monolayer. *J. Chem. Phys.* **2003,** *119*, 7461–7466.
19. Pickering, S. U. Emulsions. *J. Chem. Soc.* **1907,** 2001–2021.
20. Tohver, V.; Chan, A.; Sakurada, O.; Lewis, J. A. Nanoparticle Engineering of Complex Fluid Behavior. *Langmuir* **2001,** *17*, 8414–8421.
21. Chan, A. T.; Lewis, J. A. Electrostatically Tuned Interactions in Silica Microsphere−Polystyrene Nanoparticle Mixtures. *Langmuir* **2005,** *21*, 8576–8579.
22. Casagrande, C.; Fabre, P.; Raphael, E.; Veyssie, M. Janus Beads: Realization and Behavior at Water Oil Interfaces. *Europhys. Lett.* **1989,** *9*, 251–255.
23. Binks, B. P.; Lumsdon, S. O. Pickering Emulsions Stabilized by Monodisperse Latex Particles: Effects of Particle Size. *Langmuir* **2001,** *17*, 4540–4547.
24. Zhang, L.; Hong, L.; Yu, Y.; Bae, S. C.; Granick, S. Nanoparticle-Assisted Surface Immobilization of Phospholipid Liposomes. *J. Am. Chem. Soc.* **2006,** *128*, 9026–9027.
25. Zhang, L. F.; Granick, S. How To Stabilize Phospholipid Liposomes (Using Nanoparticles). *Nano Lett.* **2006,** *6*, 694–698.
26. Liu, J. W.; Luijten, E. Stabilization of Colloidal Suspensions by Means of Highly Charged Nanoparticles. *Phys. Rev. Lett.* **2004,** *93*, 247802-1–4.
27. Liu, J.; Luijten, E. Colloidal Stabilization *via* Nanoparticle Halo Formation. *Phys. Rev. E* **2005,** *72*, 061410-1–10.
28. *Cumulants Analysis defined in ISO13321; Calculating Volume Distribution from Dynamic Light Scattering*; Malvern Instruments, Worcestershire, UK, 2007.
29. Petelska, A. D.; Figaszewski, Z. A. Effect of pH on the Interfacial Tension of Lipid Bilayer Membrane. *Biophys. J.* **2000,** *78*, 812–817.
30. Savarala, S.; Monson, F.; Ilies, M. A.; Wunder, S. L. Supported Lipid Bilayer NanoSystems Stabilization by Undulatory-Protrusion Forces, and Destabilization by Lipid Bridging. *Langmuir* **2011,** submitted for publication.
31. Pashley, R. M. DLVO and Hydration Forces between Mica Surfaces in Li^+, Na^+, K^+, and Cs^+ Electrolyte Solutions: A Correlation of Double-Layer and Hydration Forces with Surface Cation Exchange Properties. *J. Colloid Interface Sci.* **1981,** *83*, 531–546.
32. Pashley, R. M. Hydration Forces between Mica Surfaces in Aqueous-Electrolyte Solutions. *J. Colloid Interface Sci.* **1981,** *80*, 153–162.
33. Israelachvili, J. N.; Adams, G. E. Measurement of Forces between 2 Mica Surfaces in Aqueous-Electrolyte Solutions in Range 0−100 nM. *J. Chem. Soc., Faraday Trans. 1* **1978,** *74*, 975–1001.
34. Cowley, A. C.; Fuller, N. L.; Rand, R. P.; Parsegian, V. A. Measurement of Repulsive Forces between Charged Phospholipid Bilayers. *Biochemistry* **1978,** *17*, 3163–3168.
35. Israelachvili, J. N.; Pashley, R. M. Molecular Layering of Water at Surfaces and Origin of Repulsive Hydration Forces. *Nature* **1983,** *306*, 249–250.
36. Horn, R. G.; Israelachvili, J. N.; Marra, J.; Parsegian, V. A.; Rand, R. P. Comparison of Forces Measured between Phosphatidylcholine Bilayers. *Biophys. J.* **1988,** *54*, 1185–1186.
37. Evans, E. A.; Parsegian, V. A. Thermal-Mechanical Fluctuations Enhance Repulsion between Biomolecular Layers. *Proc. Natl. Acad. Sci. U.S.A.* **1986,** *83*, 7132–7136.
38. Lipowsky, R.; Grotehans, S. Hydration *vs* Protrusion Forces between Lipid Bilayers. *Europhys. Lett.* **1993,** *23*, 599–604.
39. Barr, S. A.; Luijten, E. Effective Interactions in Mixtures of Silica Microspheres and Polystyrene Nanoparticles. *Langmuir* **2006,** *22*, 7152–7155.
40. Karanikas, S.; Louis, A. A. Dynamic Colloidal Stabilization by Nanoparticle Halos. *Phys. Rev. Lett.* **2004,** *93*, 24.
41. Zhang, F.; Long, G. G.; Jemian, P. R.; Ilavsky, J.; Milam, V. T.; Lewis, J. A. Quantitative Measurement of Nanoparticle Halo Formation around Colloidal Microspheres in Binary Mixtures. *Langmuir* **2008,** *24*, 6504–6508.
42. Hong, X. T.; Willing, G. A. Transition Force Measurement between Two Negligibly Charged Surfaces: A New Perspective on Nanoparticle Halos. *Langmuir* **2009,** *25*, 4929–4933.
43. Asakura, S.; Oosawa, F. Interaction between Particles Suspended in Solutions of Macromolecules. *J. Polym. Sci.* **1958,** *33*, 183–192.
44. Vrij, A. Polymers at Interfaces and Interactions in Colloidal Dispersions. *Pure Appl. Chem.* **1976,** *48*, 471–483.
45. Walz, J. Y.; Sharma, A. Effect of Long-Range Interactions on the Depletion Force between Colloidal Particles. *J. Colloid Interface Sci.* **1994,** *168*, 485–496.
46. Scheer, E. N.; Schweizer, K. S. Haloing, Flocculation, and Bridging in Colloid−Nanoparticle Suspensions. *J. Chem. Phys.* **2008,** *128*, 164905-1–15.
47. Roiter, Y.; Ornatska, M.; Rammohan, A. R.; Balakrishnan, J.; Heine, D. R.; Minko, S. Interaction of Nanoparticles with Lipid Membrane. *Nano Lett.* **2008,** *8*, 941–944.
48. Marsh, D. *CRC Handbook of Lipid Bilayers*; CRC Press: Boca Raton, FL, 1990.